Eddy Maintenance and Attrition in a Vertically Sheared Current under Arctic Ice

SHENN-YU CHAO

Horn Point Laboratory, University of Maryland Center for Environmental Science, Cambridge, Maryland

PING-TUNG SHAW

Department of Marine, Earth and Atmospheric Sciences, North Carolina State University, Raleigh, North Carolina

(Manuscript received 20 August 1997, in final form 24 February 1998)

ABSTRACT

Steady drift of an ice cover produces a vertically sheared current in the upper ocean of the Arctic. Under the ice cover, mesoscale shallow brine and freshening sources generate submerged anticyclones and cyclones, respectively. A submerged eddy extending deep into the water column experiences differential advections by the vertically sheared current. Interaction between subsurface eddies and the sheared current is examined using a three-dimensional numerical model in a coordinate system moving with the ice. The initial salinity field is in geostrophic balance with the sheared current, and a pulse of brine or freshening forcing produces an anticyclone or a cyclone. In a coordinate system moving with the ice, eddies are in a vertically sheared backward ambient current. To an observer looking into the direction of the backward ambient current, eddies move with the current and deflect to the right (left) for counterclockwise (clockwise) rotating eddies in both hemispheres. The lower half of the eddy always moves faster. The lateral movement can be explained by the Kutta–Zhukhovski lift theorem. Differential advection produces eddy tilting and entails the development of a narrow jet following the moving eddy. The jet reduces eddy straining and tilting, and eddies disperse in cases of sizeable tilts. Driven by a vertically sheared current, cyclones are short-lived compared with anticyclones because the lateral movement of a cyclone exposes the lower part of the eddy into waters of weaker stratification. The results help explain the predominance of anticyclonic eddies under the Arctic ice.

1. Introduction

Stratification in the surface layer of the Arctic Ocean is chiefly maintained by a shallow halocline. Salinity increases from about 30.5 psu beneath a mixed layer of 50 m or so to about 35 psu at a depth of 400 m, becoming nearly uniform at greater depths. By comparison, temperature varies little with depths. Under the ice cover of the Amerasian basin, the shallow halocline harbors a ubiquitous field of predominantly anticyclonic eddies. Their radii, typically of 5–10 km, are comparable to the first few baroclinic Rossby radii characterizing the upper-ocean stratification in the Arctic Ocean. These eddies are sufficiently small that the planetary dispersion can be safely ignored. Maximum rotational speeds within an eddy, ranging up to 60 cm s^{-1} (Galt 1967; Dixit 1978), are normally found in a depth range between 100 and 150 m. Typically, these eddies are embedded in a quiescent upper ocean having a mean circulation of a few centimeters per second. Recent estimates (Manley and Hunkins 1985) suggested that these eddies may occupy up to 25% of the surface area of the Beaufort Sea, and more than 95% of the eddies are anticyclonic.

Mechanisms leading to the predominance of anticyclones have not been identified with certainty so far, and competing theories increase in time. Most models, either numerical or conceptual, draw analogies from open-ocean eddies in ice-free conditions and involve only one moving layer. The underlying assumption is that friction exerted by the ice cover plays a secondary role. Leaving the planetary beta effect aside, D'Asaro (1988), for example, attributed the predominance of anticyclones to shear production as the seaward flow in the Chukchi Sea rubs against the coast to its right. Nof (1989) noted that the emergence of anticyclones from several closely packed eddies must follow several first principles. Cushman-Roisin and Tang (1990) suggested that, if finite-amplitude vertical displacements of the interface are allowed for a field of geostrophic turbulence, winning vortices will be mostly anticyclonic. As it stands, all these theories remain contentious, awaiting verification by using qualified high-resolution models that include friction exerted by the ice cover. For example, what

Corresponding author address: Dr. Shenn-Yu Chao, Horn Point Laboratory, University of Maryland Center for Environmental Science, P.O. Box 775, Cambridge, MD 21613-0775.
E-mail: chao.hpl.umces.edu

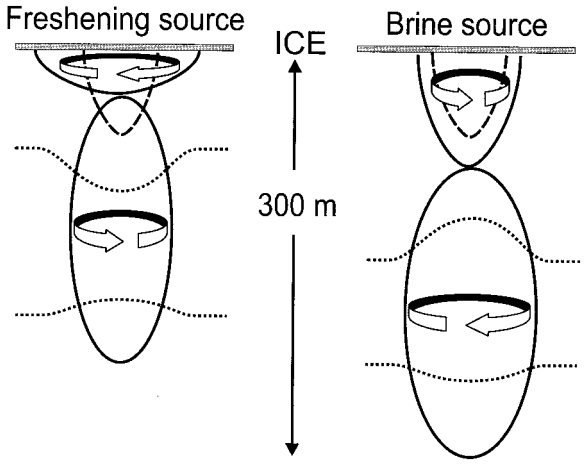

FIG. 1. A schematic sectional view showing how a freshening or a brine source in an initially quiescent ocean generates vertically stacked pairs of counterrotating eddies. Dashed contours beneath the ice cover indicate a region where a freshening or a brine source is applied. Dotted contours indicate isohalines associated with eddy pairs. Top eddies are dampened by surface friction in time.

would happen if open ocean eddies are overrun by an ice cover?

2. Our perspective

The possibility that Arctic eddies may be generated by shallow brine or freshening sources has been explored recently by Chao and Shaw (1996, hereafter CS96) using a three-dimensional numerical model with sufficient vertical resolution for the characteristic upper-ocean stratification of the Arctic Ocean. Figure 1 illustrates the outcome. The ice cover was approximated by a no-slip surface. Dashed lines indicate a shallow region where a pulse of brine or freshening source is applied. Without an ice cover, a shallow axisymmetric brine source produces a shallow cyclone with a submerged anticyclone beneath the cyclone. With the presence of the ice cover, the surface stress exerted by the ice damps off the top cyclone and leaves the submerged anticyclone in sole existence. Conversely, a shallow freshening source generates a shallow anticyclone and a submerged cyclone below; surface stress is able to annihilate the top anticyclone and leaves the submerged cyclone intact. The eddies are mainly confined within a shallow halocline. Isohalines (dotted lines) within a submerged anticyclone are displaced away from a horizontal surface, while those within a submerged cyclone are pinched toward that surface. The model-produced submerged anticyclones and cyclones have many attributes similar to those observed. Since fresher waters rise and spread while saline waters sink and converge during the spinup period, the eddy pair produced by a freshening source is shallower and weaker than that induced by a brine source of comparable strength. The disparity would vanish in linear models, as both adjustments to scales of the Rossby radius are similar to the geostrophic adjustment problem. What distinguishes the two is the downward convection induced by the brine source, deepening and strengthening the top cyclone and submerged anticyclone.

The ice cover absorbs oceanic heat and releases brine in winter; it also contributes freshwater to the surface layer in summer. Brine is expected to form sinking plumes that are rich in mesoscale variability. A freshwater surface layer, on the other hand, should remain as a shallow, expansive buoyant layer with little mesoscale variability. From these considerations, CS96 suggested that the predominance of anticyclones under Arctic ice may be primarily caused by shallow brine sources. Shallowness is the key to the whole argument. If a deep brine source is applied, the surface cyclone will be too deep to be dissipated by surface friction. The overall agreement with observations inspires confidence that the basic idea can be tested further in a more realistic setting.

The next order of importance, in our view, is to take into account the effect of the ice drift. When ice moves, the ridge keel stirs and transfers momentum from the ice to the ocean. A vertically sheared current should be generated. Its velocity equals that of the ice drift at the ocean–ice interface and vanishes at some depth beneath the ice. The depth of the sheared layer depends of course on the form drag exerted by the ice. If the sheared layer is shallow, vertical friction should balance the momentum input from the moving ice cover. In deeper sheared layers, the current should be geostrophically balanced by lateral tilts of isopycnals. Observations in the Beaufort Sea support the latter scenario; the overall anticyclonic ice drift correlates well with the mean dynamic topography between 30 and 300 decibars (Newton 1973). To an observer moving with the ice, the submerged eddy generated by a brine or freshening source should experience a back sheared current relative to the ice drift. This current increases with depths and becomes constant below a sheared layer. Effect of this current on submerged eddies is investigated in this paper.

Eddies generated by brine or freshening sources under drifting ice experience no force if the entire ocean moves with the same speed as the ice. To an observer stationed on the ice, the ocean is motionless, and eddies are spun up in an otherwise quiescent ocean. The uniform translation scenario can be violated. First, if there is a sudden velocity change in the ice–ocean system, the ice-based observer notes a suddenly imposed uniform current acting on the initially stationary eddy. In this case, the eddy may move both with the current and laterally. Furthermore, if the speed of water movement decreases with depth, the developing eddy experiences a varying ambient current as it extends downward. Relative to the ice-based observer, the current is in a direction opposite to the ice drift. Its speed increases downward and levels off to that of the ice drift at greater depths. Thus, the eddy will not only move backward and laterally relative

to the ice, but also experience a shearing stress due to differential advection at different depths. Speculation about eddy movements in a suddenly imposed, vertically sheared current is considered below.

Consider a circular eddy held steady in space in a layer of barotropic fluid moving at a vertically uniform speed V_0. To find forces acting on the eddy, analogy can be drawn from a well-known theory governing potential flows past a circular cylinder with circulation Γ around it (e.g., Kundu 1990, 156–159). Let the fluid density be ρ. The Kutta–Zhukhovski lift theorem suggests that the cylinder should experience a lift force $L = \rho V_0 \Gamma$, transverse to the incoming flow. The lateral lift follows the conservation of Bernoulli function $B = P/\rho + V^2/2$, where P is pressure and V is flow speed. Along the cylinder diameter transverse to the ambient current, the incoming flow makes the swirling speed low on one side and high on the other. Pressure is high on the side of low speed and low on the side of high speed. The lateral pressure gradient force produces the lift. Facing downstream the lift force is toward the left (right) for a clockwise (anticlockwise) rotating cylinder. If not held steady in space, the cylinder drifts laterally while moving with the ambient current.

The vertical shear of the ambient current complicates the situation. Differential advection is likely to displace the upper and lower parts of an eddy differently. If the Kutta–Zhukhovski lift theorem holds strictly on a layer-by-layer basis, the differential advection in the vertical entails eddy disintegration and destruction. Regardless of the ice drift speed, continuous straining will eventually distort the eddy beyond recognition. This argument must have overestimated the ability of a vertically sheared current to annihilate submerged eddies, as the observed abundance of eddies under Arctic ice suggests otherwise. In the nonlinear, baroclinic, rotating regime, secondary circulation must develop somehow to hold a vertically displaced eddy together against the destruction by a vertically sheared ambient current. Numerical experiments to be discussed below are designed to seek answers to this issue.

The remainder of this paper is organized as follows. The numerical model is formulated in section 3. Numerical results are discussed in four parts in section 4. Vertical features of subsurface eddies without an ice drift are given in 4a. Section 4b discusses trajectories of submerged eddies in vertically sheared currents. Consequences of interaction between anticyclones and a sheared flow are given in section 4c. Section 4d discusses how cyclones interact with a vertically sheared current. Numerical results are interpreted in section 5. Section 6 puts major findings in proper perspectives.

3. Model formulation

Figure 2 depicts the system to be investigated. In the land-based frame (x', y', z'), a steady ice drift with a uniform speed U_0 along the x' axis generates a vertically

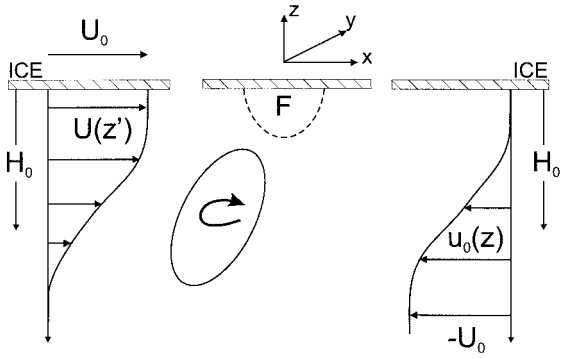

FIG. 2. Side view of an eddy in a coordinate system moving with the ice cover at speed U_0. The current profiles in the ice- and land-based coordinate systems are shown on the right and left, respectively. The eddy is generated beneath the source F. When being swept backward, an anticyclone (cyclone) tilts and moves laterally toward the $-y$ ($+y$) direction in the Northern Hemisphere with the lower part of the eddy leading. In this illustration the submerged eddy is anticyclonic; the lower part of the eddy should be displaced out of the paper.

sheared ambient current in the upper ocean. The sheared current having a depth scale H_0 is approximated by

$$U(z') = U_0 \exp(-z'^2/H_0^2) \tag{1}$$

A shallow brine or freshening source F is imposed in a finite volume centered around the origin of the frame (x, y, z) moving with the ice. The ambient current, which perturbs the submerged eddy generated below the source, is

$$u_0(z) = U(z) - U_0 \tag{2}$$

in the moving frame. Positive x and y directions will be referred to as east and north, respectively. The fixation is artificial; horizontal axes of the model can be rotated without loss of generality. If the ice drift produces an eastward geostrophic current in the Northern Hemisphere, sea level rises to the south.

The ocean model is hydrostatic and Boussinesq with a reference density ρ_0. The Coriolis parameter f is fixed at a constant value of 1.4×10^{-4} s^{-1}. Let (u', v', w') be velocity in the (x', y', z') frame. Transformation from the land-based reference frame to the ice-based frame follows the rules $(x, y, z, t) = (x' - U_0 t, y', z', t')$ and $(u, v, w) = (u' - U_0, v', w')$. From the chain rules $\partial/\partial(x', y', z') = \partial/\partial(x, y, z)$ and $\partial/\partial t' = \partial/\partial t - U_0 \partial/\partial x$, the governing equations in the ice-based frame become

$$\frac{Du}{Dt} - fv = -\frac{1}{\rho_0}\frac{\partial P}{\partial x} + \nabla_H \cdot (A\nabla_H u) + \frac{\partial}{\partial z}\left(\nu \frac{\partial u}{\partial z}\right) \tag{3a}$$

$$\frac{Dv}{Dt} + fu = -\frac{1}{\rho_0}\frac{\partial P}{\partial y} + \nabla_H \cdot (A\nabla_H v) + \frac{\partial}{\partial z}\left(\nu \frac{\partial v}{\partial z}\right) \tag{3b}$$

$$\frac{\partial P}{\partial z} = -g\rho \tag{3c}$$

$$\frac{\partial u}{\partial x} + \frac{\partial v}{\partial y} + \frac{\partial w}{\partial z} = 0, \tag{3d}$$

TABLE 1. List of numerical experiments. The A and C represent submerged anticyclones and cyclones, respectively. Experiments A0, C0, and C0D establish reference solutions with no ice drift.

Expt	Δ_t (psu/day)	z_0 (m)	U_0 (cm s^{-1})	H_0 (m)	y_0 (km)	Description
A0	7	50	0	—	0	Anticyclone; no ice drift
C0	−7	50	0	—	0	Cyclone; no ice drift
C0D	−3.5	150	0	—	0	Deeper cyclone; no ice drift
A1	7	50	10	200	0	Normal halocline; stable anticyclone
A2	7	50	10	200	−80	Weak halocline; anticyclone destroyed
A3	7	50	10	100	0	Shallow shear layer; stable anticyclone
A4	7	50	15	200	0	Fast ice drift; anticyclone destroyed
A5	3.5	50	10	200	0	Stable, weak anticyclone
C1	−7	50	10	200	0	Normal halocline; cyclone destroyed
C2	−7	50	10	200	−80	Weak halocline; cyclone destroyed
C3	−3.5	150	10	200	0	Normal halocline; deeper cyclone destroyed

where g is the gravitational constant, and (A, ν) are the horizontal eddy viscosity and the vertical momentum mixing coefficient, respectively. In (3), a sea surface pressure component, $-\rho_0 f U_0 y$ in geostrophic balance with U_0, has been subtracted from the pressure field P. Density ρ is related to salinity by $\rho = \rho_0(1 + \alpha S)$, where $\alpha = 8 \times 10^{-4}$ (psu)$^{-1}$. The Arctic Ocean is nearly isothermal in the vertical, so the temperature equation is therefore neglected in this model. Salinity is governed by

$$\frac{DS}{Dt} = \nabla_H(K\nabla_H S) + \frac{\partial}{\partial z}\left(\kappa\frac{\partial S}{\partial z}\right) + F, \tag{4}$$

where (K, κ) are the horizontal diffusivity and the vertical mixing coefficient for salt. The source term F is given by

$$F = \Delta_t \exp\left(-\frac{x^2 + y^2}{b^2} - \frac{z^6}{z_0^6}\right). \tag{5}$$

The salinity forcing has an e-folding radius $b = 8$ km and a depth scale (z_0) of either 50 or 150 m. The source strength Δ_t in units of psu per day is given in Table 1. The source is applied for a finite duration of one day to produce a sizeable submerged eddy. The moving reference frame has the advantage of fixing the center of salinity forcing at the origin of an x–y plane and is in keeping with the fact that most of the submerged eddies are observed from ice-based stations.

In the moving reference frame, the initial velocity is $(u, v, w) = (u_0(z), 0, 0)$. The initial salinity field contains two components: $S(y, z, t = 0) = S_0(z) + S_1(y, z)$. The characteristic halocline of the Arctic Ocean is represented in psu by $S_0(z) = 30.5 - 4.5 \tanh(z/Z)$, where $Z = 500$ m. The sheared current $u_0(z)$ is in thermal wind balance with $S_1(y, z)$ so that

$$S_1(y, z) = \frac{f}{g\alpha}\frac{du_0}{dz}(y - y_0), \tag{6}$$

where y_0 is an unspecified constant. The buoyancy frequency N is given by

$$N^2 = -g\alpha\frac{dS_0}{dz} - f\frac{d^2u_0}{dz^2}(y - y_0). \tag{7}$$

If $d^2u_0/dz^2 = 0$, N^2 is independent of y. For the current profile (2), N^2 increases (decreases) linearly with y above (below) $z = H_0 2^{-1/2}$, the depth of the maximum velocity shear. The first baroclinic Rossby radius for the stratification is 19.2 km, about twice of the e-folding radius of the salinity forcing ($b = 8$ km).

The numerical model follows that of Blumberg and Mellor (1987). The primitive equation model is preferred to a quasigeostrophic model because it copes much better with large vertical isohaline displacements generated by salinity forcing within one Rossby radius. The vertical mixing coefficients (ν and κ) are determined by a level-2.5 turbulence closure scheme (Mellor and Yamada 1974). A turbulent parameterization scheme is needed to dampen the top eddy of a vertically stacked pair. In this light, the model is insensitive to the particular turbulent closure scheme chosen. Once the top eddy is eliminated, interactions of the submerged eddy with ambient flow involve much less dissipation. The horizontal eddy viscosity depends on the local flow shear and divergence as in Smagorinsky (1963):

$$A = 0.1\Delta^2\left[\left(\frac{\partial u}{\partial x}\right)^2 + \left(\frac{\partial v}{\partial y}\right)^2 + 0.5\left(\frac{\partial v}{\partial x} + \frac{\partial u}{\partial y}\right)^2\right],$$

where $\Delta = 2$ km is the horizontal grid spacing, and the horizontal eddy diffusivity is $K = 0.2A$. Save for small sea level fluctuations, the model basin has a uniform depth of 4 km in 41 layers. The deepest layer is 405 m thick, while the thickness of each layer above the bottom layer is 0.9 of that immediately below. Excluding the small sea level fluctuation, the top layer is 6 m thick. The sea level is free to oscillate about a leveled mean sea surface, noting that a mean sea level slope in the meridional direction has been removed through transformation from a stationary to a moving frame. Further, the deep and flat basin is used to investigate eddy movements free from bottom topographic variations.

The basin is 160 km long and 160 km wide. Boundary conditions are as follows. The basin is cyclical in the x direction. Laterally, the initial salinity field increases linearly in y and therefore disallows cyclic boundary conditions. Instead, the gradients of all dependent variables vanish on the northern and southern boundaries. It is important to keep the north and south boundaries open. If the two boundaries are replaced by vertical walls, inertial oscillations will outgrow the mean current in time. In the moving reference frame the surface boundary is no-slip, impermeable and impenetrable. To a land-based observer, the ice cover is seen as a rigid plate drifting with the ambient surface current, unable to be deformed by submerged eddy activities below. This is the limit of a highly compacted ice cover. Further, an Ekman spiral in the upper ocean is neglected in the initial condition, but is allowed to evolve subsequently. In the depth range of interest to us, the Ekman veering is not particularly noticeable from model results. The bottom boundary conditions are similar except that the no-slip condition is replaced by a free-slip one. The model ocean is spun up from the initial thermal wind balance. In the first model day, no brine or freshening source is imposed, allowing weak inertial oscillations to dissipate. The brine or freshening source is turned on for the second day and switched off thereafter. A submerged eddy thus generated is subject to advection by the vertically sheared current for 18 days. The numerical model employs a mode-splitting technique to resolve external and internal modes with different time steps. The time step is 160 s for the internal mode and 2 s for the external mode.

4. Numerical results

Submerged anticyclones and cyclones are first made comparable in strength and dimension before they are subject to external forcing of the vertically sheared current (2). Using salinity sources of the same magnitude but of opposite signs produce a cyclone and an anticyclone of comparable sizes and strength, but the resulting cyclone has a much elevated core. To ''level the playing field,'' one could choose a weaker and deeper freshening source to produce a submerged cyclone. The core strength and depth of the submerged cyclone produced this way are closer to those of a submerged anticyclone induced by a shallower but stronger brine source.

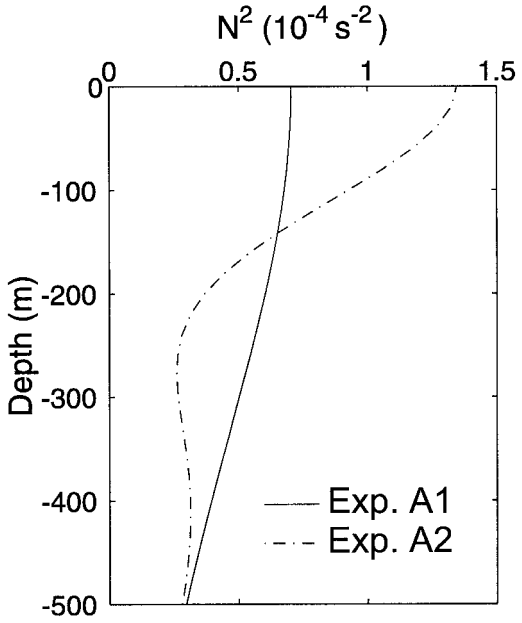

FIG. 3. Profiles of N^2 at the center latitude of the basin for experiments A1 and A2. Since N^2 varies linearly with y at a fixed depth, difference between the two profiles remains at all other latitudes. Specifically, stratification below 140-m depth is always stronger in A1 than in A2.

Table 1 summarizes the experiments discussed in this paper. Experiments A0 and C0 establish vertical features of a submerged anticyclone and a submerged cyclone in the absence of a vertically sheared current. The two submerged eddies are produced, respectively, by a brine source and a freshening source of equal depth scale ($z_0 = 50$ m) and strength ($|\Delta_t| = 7$ psu/day). The resulting cyclone C0 is comparable to anticyclone A0 in dimension and strength, but the core depth is much elevated. In experiment C0D, a submerged cyclone is produced by a deeper ($z_0 = 150$ m) but weaker ($\Delta_t = -3.5$ psu/day) freshening source, deepening the core of the submerged cyclone to a level comparable to that of a submerged anticyclone produced in experiment A0.

Including a vertically sheared current, experiments A1 and A2 describe the behavior of a submerged anticyclone similar to that in A0 in waters of different stratification. The upper-ocean stratification can be adjusted by varying the latitude (y_0) in the thermal wind equations (6) and (7) since the stratification varies linearly with $y - y_0$ at a fixed depth. Figure 3 shows N^2 profiles for experiments A1 and A2 at the center latitude of the basin. The stratification below the maximum velocity shear (140 m) is stronger in experiment A1 than in experiment A2 because y_0 is shifted 80 km southward in A2. The difference remains at all other latitudes since N^2 varies linearly with $y - y_0$ at any given depth. In reference to A1, experiment A3 or A4 examines the

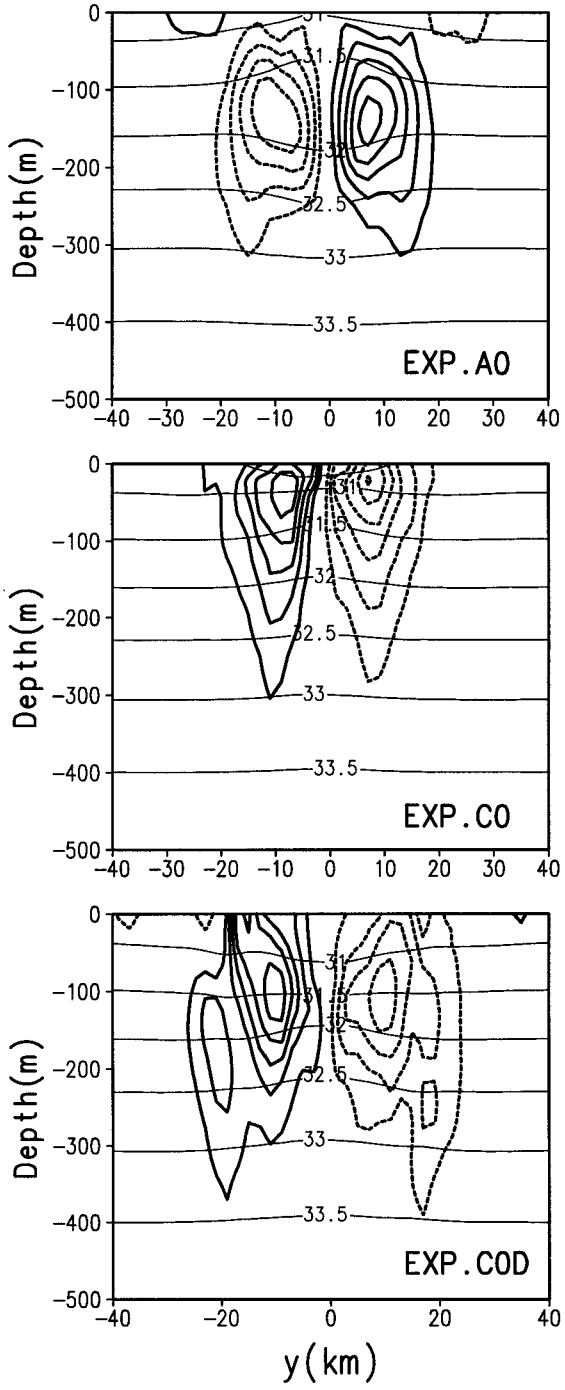

FIG. 4. Salinity in psu (thin lines) and azimuthal velocity (thick lines) in the *y*–*z* plane at day 20 in experiments A0 (top), C0 (middle), and C0D (bottom). Dashed and solid isotachs are into and out of the paper, respectively, with the outermost isotachs at ± 2 cm s^{-1} and a contour interval of 2 cm s^{-1}.

same anticyclone in a shallower sheared layer or with a faster ice drift, and anticyclone A5 is weaker. Experiments C1 and C2 are similar to A1 and A2, respectively, but describe the submerged cyclone C0 in a vertically sheared current. Cyclones C1 and C2 have unrealistically shallow cores and are short-lived. By employing the deeper and weaker freshening source in experiment C0D, the submerged cyclone C3 has a realistic core depth and greater survivability in the vertically sheared current.

a. Submerged eddies with no ice drift

Vertical features of the submerged anticyclone (A0) and submerged cyclones (C0 and C0D) without an ice drift are briefly summarized below, reiterating main conclusions from CS96. These three cases represent an ocean-ice system either being stationary ($U_0 = 0$) or moving with uniform speed relative to land ($H_0 \to \infty$). Figure 4 shows *y*–*z* sections of salinity and azimuthal velocity at day 20. A brine source generates positive density anomaly, downwelling, and cyclonic rotation near the surface. Beneath the shallow cyclone, pressure becomes higher in the eddy because of the added weight of the brine. The pressure imbalance generates radially outward flow and downward motion, which depresses isohalines at depths and produces a density deficit relative to the surrounding water. This process produces doming of shallow isopycnals and depression of isopycnals below. Further, Coriolis deflection of the radially outward flow beneath the top cyclone produces an anticyclone. The pair of vertically aligned, counterrotating eddies exists only in open waters. Under the ice cover, friction exerted by ice dampens the top cyclone while leaving the lower anticyclone intact. Figure 4a shows the surviving anticyclone centered at 130-m depth with a maximum rotation speed of 10 cm s^{-1} and isohalines displaced away from this depth. These are the telling features of submerged anticyclones under the Arctic ice.

Conversely, a freshening source generates an upper anticyclone and a lower cyclone. The top anticyclone is eliminated by surface stress exerted by ice, and the submerged cyclone is brought to sole existence (Figs. 4b,c). Upwelling and radially inward motion at depths produce the submerged cyclone. Upwelling also elevates the core of the submerged cyclone to a shallower depth. In experiment C0, the freshening source has the same strength and structure as the brine source in experiment A0, but isohalines are pinched toward a core depth of 30 m. In experiment C0D, isohalines associated with the submerged cyclone are pinched toward a lower and more realistic depth of 120 m by using a weaker source extending to 150 m.

Eddies as shown in Fig. 4 are more geostrophic than cyclostrophic. At a radial distance of 10 km, the swirling speed at the core is about 10 cm s^{-1}. Thus, the Coriolis force is about 14 times larger than the centrifugal force at the core of maximum rotation speeds.

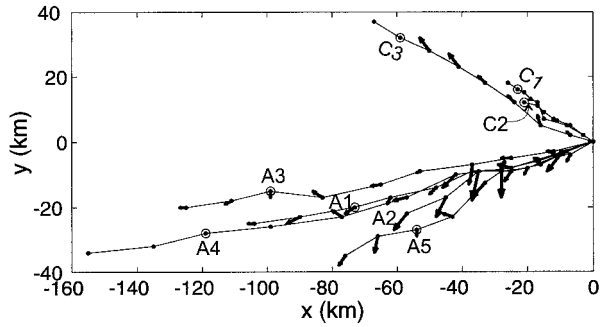

FIG. 5. Trajectories of centers of submerged anticyclones and cyclones at 100 m in a frame moving with the ice cover. Adjacent dots in a track are separated by two days and the 16th day mark is enclosed in a circle. Arrows show the relative displacement of the eddy center at 200 m with respect to that at 100 m. Tracks shorter than 20 days indicate eddy dispersal. Coordinates are in reference to the initial center of salinity forcing, which is placed at origin.

b. Tracks of eddies in a sheared flow

Eddy location, as determined by closed isohalines at a constant depth, is plotted at the 100-m depth at intervals of two days in the ice-based coordinate system (Fig. 5). This is the depth of the density surplus or deficit in the upper part of the eddy in experiments A1–5 and C3. In experiments C1 and C2, the upper part of the eddy is subject to excessive friction exerted by the ice cover and diffuses away quickly; only the lower portion of the eddy at 100-m depth can be tracked with certainty for some time. Therefore, the trajectories of cyclones C1 and C2 show the position of the lower part. Eddies tilt as they drift. To quantify the tilt better, eddy centers at 200 m, when existing, are shown by vectors relative to their 100-m locations in Fig. 5.

Eddy structures embedded in an ambient current will be illustrated later. Some elements, to be substantiated later, are invoked in advance to elucidate eddy movements. Because of the drag force from the ice, anticyclone A1 moves in the direction of the ice drift but at a slower speed and deflects to the south in the land-coordinate system. Relative to the steady ice drift, the eddy is in a backward ambient current in the negative x direction. In the ice-based frame, the rotational speed of eddy A1 is lower on the north side than on the south side. Thus, an anticyclone deflects to the south according to the Bernoulli theorem. The southwestward displacement of the eddy at 200 m relative to 100 m shows a faster backward and lateral drift for the lower portion of the eddy. Since the lower part of the eddy is embedded in a swifter backward current relative to the ice, the pressure gradient is stronger and so is the lift. The southwestward drift and tilting of eddy A1 lend support to the scenario based on the Kutta–Zhukhovski lift theorem.

Cyclone C3 has a trajectory similar to A1 except that C3 moves slower in the ice-based frame. Cyclone C3 is also less stable. As illustrated in Fig. 10, closed isohalines on constant depth surfaces can no longer be found at the later part of the trajectory. The lower part of cyclone C3 is annihilated after day 14, while the upper part continues in sole existence until day 18. Otherwise, cyclone C3 behaves much like a mirror image of A1 according to the Kutta–Zhukhovski lift theorem. The shallower cyclones C1 and C2 are both short lived. With an elevated core, the two eddies are annihilated by day 18. These eddies drift much slower than the deeper eddy C3, and the lateral movement decreases proportionally.

Each of the other experiments in Table 1 brings out a new factor regulating the eddy movement. Stratification, eddy strength, and depth of the sheared flow modify the eddy movement only quantitatively. All eddies move in the direction predicted by the Kutta–Zhukhovski lift theorem. Increasing the ice drifting speed in experiment A4 speeds up the backward motion and the lateral drift proportionally. A faster ice drift destabilizes the eddy. The lower part of submerged anticyclone A4 is destroyed after day 12 because it experiences faster ambient currents, and the upper part is in sole existence afterward. The ratio of the lateral displacement to the downstream displacement is different in A2, A3, and A5. In experiment A3, the eddy extends beneath the shallow sheared layer and experiences a swifter backward current relative to ice with less vertical shear. The eddy moves faster in the backward direction, but the lateral movement and the tilt are both reduced. In experiment A2, the speed of downstream motion is similar to that in A1, but changing the upper-ocean stratification produces a faster lateral drift in the ice-based frame and a more enhanced eddy tilt. The eddy is also less stable. The eddy at 100 m is no longer recognizable after day 14, and the bottom portion is destroyed after day 16. In experiment A5, a weaker anticyclone is produced by a weaker brine source. Relative to the ice cover, the backward movement of the eddy becomes slower but the lateral drift is faster. Eddy tilt is also enhanced. It seems that differential advection is stronger with a weak salinity gradient below the sheared layer and for weak eddies.

Eddy tilting indicates differential advection with depth. Shearing of an eddy usually results in quick eddy dispersal. However, differential advection has its limitation. In all cases, the continuous straining does not separate the upper and lower portions of an eddy immediately. Instead, a secondary circulation seems to develop to hold the eddy together. While the lower part of an eddy drifts at a speed lower than the prevailing flow, the upper part of the eddy accelerates to catch up with the lower portion. The development of the secondary circulation and how it maintains or fails to maintain the eddy circulation are discussed below.

c. Interaction of anticyclones with a vertically sheared flow

Experiments A1 and A2 are illustrated below for their generality. The two anticyclones are almost identical

initially and are subsequently advected by the same vertically sheared current for 18 days. Figure 6 shows the flow and salinity fields for experiment A1 at days 2, 10, and 20. Since the anticyclone tilts as it moves, plane features for the upper-level high (a density surplus) and lower-level low (a density deficit) for the eddy are displayed at 100-m and 200-m depths, respectively. The eddy enters the east side of the domain at day 20 because of the cyclical boundary condition. Note that only the area near the eddy is plotted in Fig. 6. Moving southwestward relative to the ice, the anticyclonic circulation intensifies, and the eddy grows larger. Flattening of the isopycnals bounding the anticyclone releases potential energy and may have contributed to the flow intensification. The eddy would not intensify and expand to such a degree without the vertically sheared current; this is clear from the top panel of Fig. 4. Not so obvious from Fig. 6 is eddy tilting. The eddy center is normally slightly displaced to the southwest at 200-m depth.

The difference in flow speeds across the eddy is larger than anticipated. The westward ambient flow relative to the ice is 2.2 cm s^{-1} at 100-m depth and 6.3 cm s^{-1} at 200-m depth following (2). Linear superposition of this ambient flow to the eddy velocity field would give a difference of 4.4 cm s^{-1} for speeds at the north and south sides of the eddy at a depth of 100 m and 12.6 cm s^{-1} at 200 m. Estimates from Fig. 6 are far greater. At day 20, for example, the difference in speeds at the north and south sides is 15 cm s^{-1} at 100-m depth and 20 cm s^{-1} at 200-m depth. Conceivably, the difference in speeds can produce a significant southward pressure gradient force. Ignoring baroclinic forcing and flow divergence, the Bernoulli's principle would suggest a southward acceleration of 11 cm s^{-1} per day if flow speeds are 20 and 5 cm s^{-1} on the southern and northern sides of the eddy, respectively. In Fig. 6, a southward jet develops behind the moving eddy. The jet is more visible at 100-m depth at day 20 and can be regarded as a ''wake'' of the eddy, following the anticyclone southwestward.

Figure 7 shows comparable features for experiment A2 at days 4, 12, and 20. In this case the eddy did not survive the 18-day journey. A southwestward tilt of the eddy with depth is visible before the eddy is annihilated. At day 12, the southward jet trailing behind the anticyclone is better developed than in experiment A1, allowing for a full view, especially at 100-m depth. The southward jet ends by developing a mushroomlike flow pattern following the movement of the eddy, with return northward flows on both sides of the jet. The northward recirculation is much stronger and extensive behind (east of) the eddy than ahead (west) of the eddy. The southward jet and the return flows are much larger in scale than the eddy itself. At day 20, the anticyclone has been completely annihilated, but the southward jet and return flows on both sides still persist, moving westward with the ambient current.

A trough, indicated by a southward excursion of isohalines, is apparently generated by the southward jet. Here a trough and a crest refer to southward and northward excursions of isolines, respectively. The trough at 100-m depth leads, or appears to the west of, that at 200-m depth. This is seemingly at odds with the downward increase of the westward ambient flow. The unexpected tilt of the trough with depths is caused by the presence of the anticyclone at early times. The submerged anticyclone is associated with an upper-level trough and a lower-level crest embedded in otherwise zonal isohalines. At 200-m depth, the trough associated with the southward jet is displaced by the crest associated with the eddy to a location behind the moving anticyclone. The backward tilt of the trough associated with the southward jet against the background current shear persists long after the eddy dissipation.

Vertical motions associated with moving anticyclones are illustrated below. Figure 8 shows closeups of vertical velocity fields in relation to salinity and horizontal flow fields for experiment A1 at day 20 (top) and A2 at day 12 (bottom). The horizontal flow and salinity fields are displayed at 100-m depth, while vertical velocity contours are shown at 200 m. The stratification at 200-m depth is stronger in A1 than in A2; vertical motions in A1 are partially inhibited by a stronger stratification and display patchiness. Leaving patchiness aside, vertical velocity fields are quite coherent vertically, peaking at around 200-m depth. Figure 8 shows that the southward jet following the moving anticyclone is associated with downwelling speeds higher than 0.01 cm s^{-1}. The downwelling is preferably under the region where the southward jet ends. Downward vertical velocity is patchy in experiment A1 (top panel) but strong and expansive in experiment A2 (bottom panel) with a weaker salinity gradient below the sheared layer. The mechanism leading to downwelling is clear. Because the salinity field is in geostrophic balance with the ambient sheared current, waters to the north are heavier than that to the south at the same depth. Heavier waters are forced to enter increasingly lighter waters to the south by the southward jet, and downwells as density contrast increases. In all experiments, downwelling is found to intensify if the speed and north–south span of the southward jet increase. The result lends support to the foregoing interpretation.

The emerging southward jet often outgrows the ambient current especially at 100-m depth. Usually, the southward jet intensifies as the lateral tilt of an eddy becomes more pronounced. Such a large perturbation is, of course, beyond the range of validity of the Kutta–Zhukhovski lift theorem. Several unexplained but minor deviations of eddy tracks could be conceivably caused by the development of a finite-amplitude jet. In experiment A3, the vertically sheared current is shallower, and the anticyclone is advected by an ambient current more uniformly in the vertical. The lateral tilt is reduced along with the southward jet. The slower southward movement seems like a consequence of a weak south-

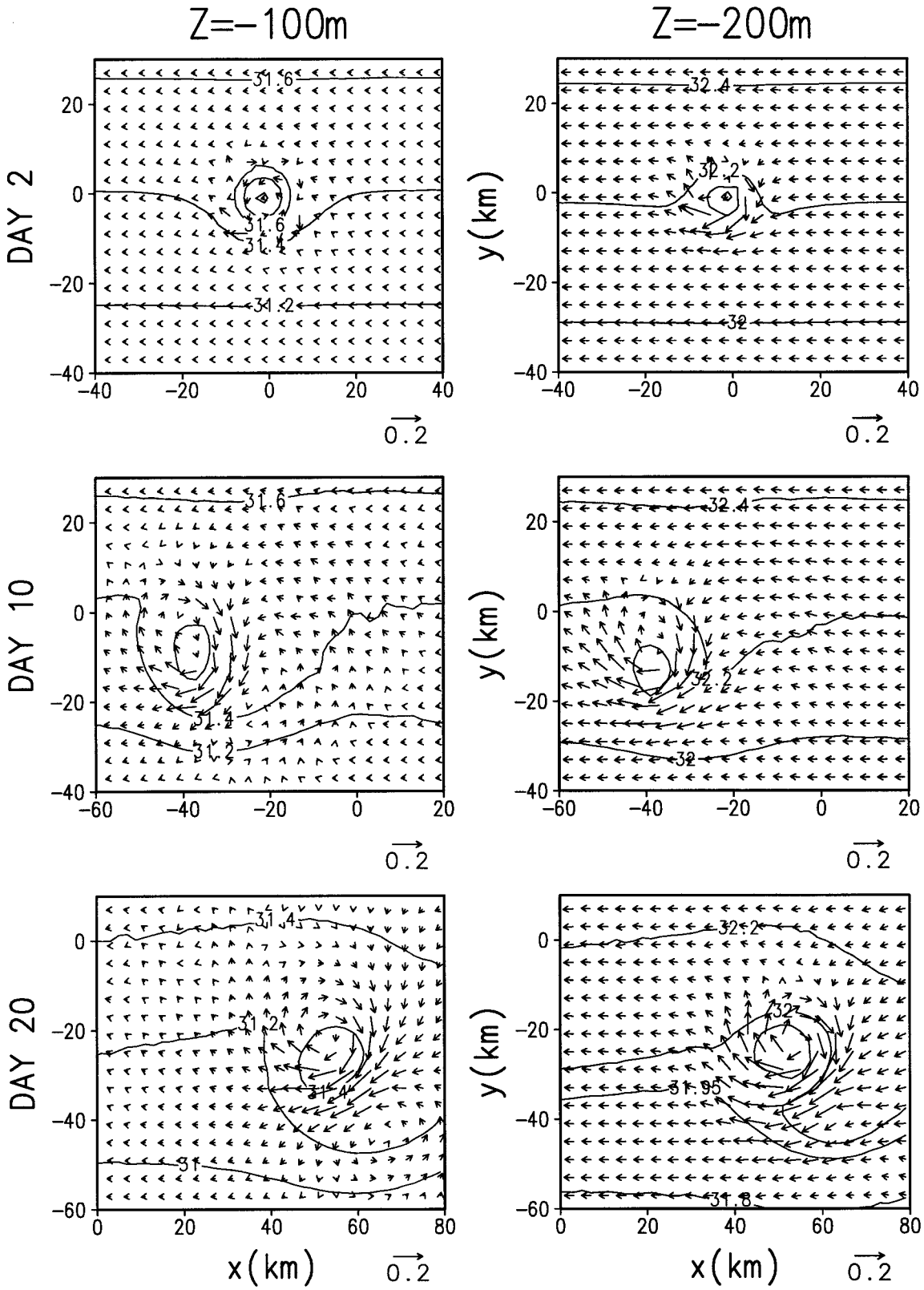

FIG. 6. Flow and salinity (psu) fields near anticyclone A1 at $z = -100$ m (left) and -200 m (right) at day 2 (top), day 10 (middle), and day 20 (bottom) in the frame moving with the ice cover. The calibration arrow for velocity is 0.2 m s^{-1}.

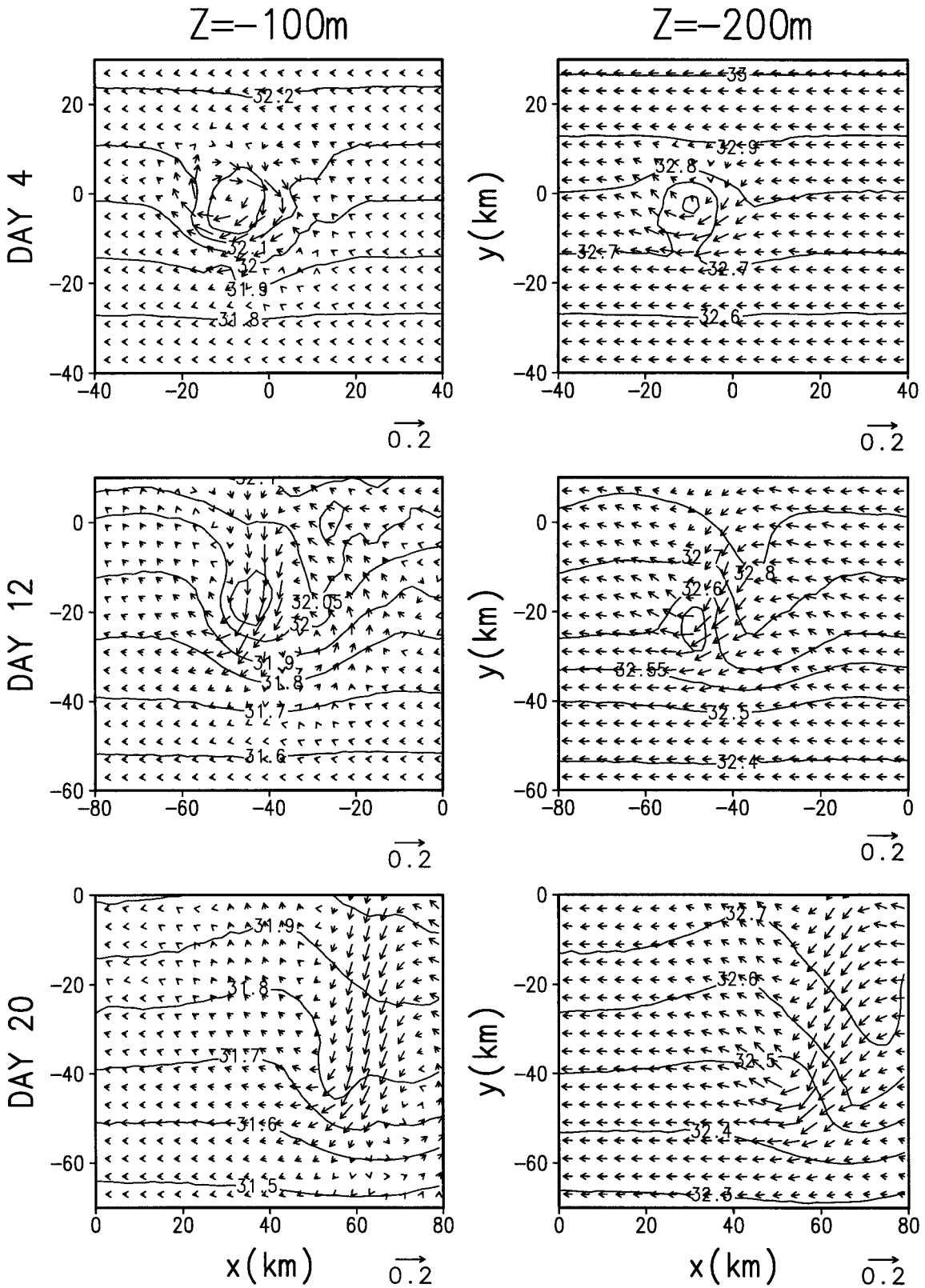

FIG. 7. Same as Fig. 6 except for anticyclone A2 at days 4, 12, and 20.

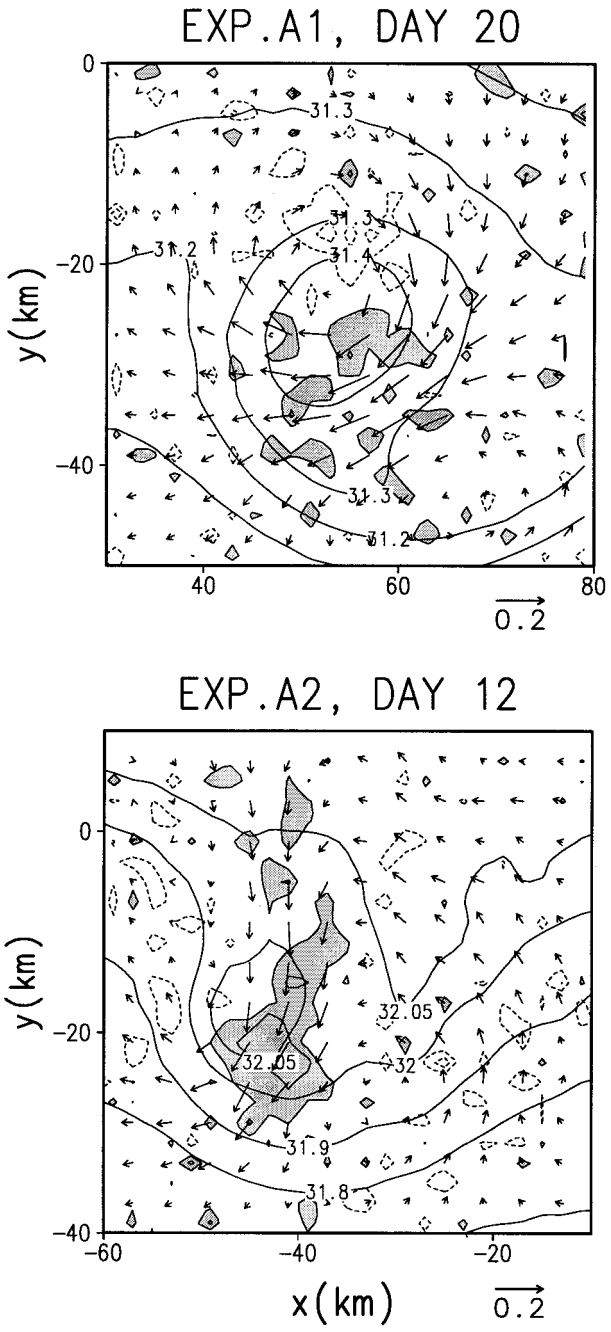

FIG. 8. Vertical velocity at $z = -200$ m superimposed on salinity (psu) and horizontal flow fields at 100 m for anticyclones A1 at day 20 (top) and A2 at day 12 (bottom). Solid contour lines show $w = -0.01$ and -0.02 cm s^{-1}, and dashed contour lines indicate $w = 0.01$ and 0.02 cm s^{-1}. Shading indicates downwelling speeds greater than 0.01 cm s^{-1}. Calibration arrow for horizontal flow is 0.2 m s^{-1}.

ward jet. In experiment A5, the weaker anticyclone is subject to stronger dispersion by the vertically sheared current. Faster lateral drift, larger lateral tilt of the eddy, and a stronger southward jet follow. In essence, the Kutta–Zhukhovski lift theorem holds to the lowest order. In a vertically sheared current, lateral tilt of an anticyclone and the consequent development of a southward jet present sizeable departures from the simple theorem. All these lateral effects seem to grow at the expense of the downstream movement of the eddy. A large lateral displacement is usually associated with slower eddy movement with the ambient current and signals eddy dispersal a few days later.

d. Interaction of cyclones with a vertically sheared flow

Figure 9 shows flow and salinity fields for experiment C1 at days 4, 12, and 20. Because of its elevated core, plane features for the upper-level low (a density deficit) and lower-level high (a density surplus) of the cyclone are displayed at 40-m and 100-m depths, respectively. The upper-level low experiences excessive friction exerted by the ice cover and diffuses away in time. Its northwestward movement can be traced up to day 12, leaving behind patches of density anomalies. The lower-level high also diminishes in time along its track northwestward. At day 20, the cyclone has dispersed and becomes a depression near $x = -30$ km and $y = 20$ km at 100-m depth.

With a deeper core, cyclone C3 provides a much clearer picture of processes at work. Figure 10 shows features in the vicinity of the eddy at days 4, 12, and 20; upper and lower parts of the cyclone are displayed at 100-m and 200-m depths, respectively. At 100-m depth, the upper part of the cyclone moves northwestward, producing a shallow anticyclone near the initial position of the cyclone. The newly created anticyclone is shallow and therefore not advected by the swifter current below, dissipating slowly near its birth location. The cyclone tilts as it moves; the lower part of the eddy consistently leads the way along the northwestward track. The tilted cyclone in motion is followed by a northward jet. Southward return flows are on both sides of the northward jet and drift with the cyclone. Other than the production of a shallow anticyclone, the overall circulation associated with the northwestward moving cyclone is a mirror image of the southwestward moving anticyclone with respect to the x axis (Fig. 6). The difference is in the details. In a comparable sheared current and halocline, the southwestward moving anticyclone is expected to survive longer than a comparable cyclone moving northwestward.

The vertical velocity in relation to horizontal current and salinity fields is shown for cyclone C3 at day 12 (Fig. 11). Salinity and horizontal flow fields are displayed at 100-m depth, while the vertical velocity is contoured at 200-m depth with shading indicating upwelling speeds higher than 0.01 cm s^{-1}. Vertical velocity is coherent in the vertical, peaking around 200-m depth as before. The northward jet transports light water from the south and induces upwelling, while the southward return flows on both sides of the eddy transport heavy water southward and produces downwelling.

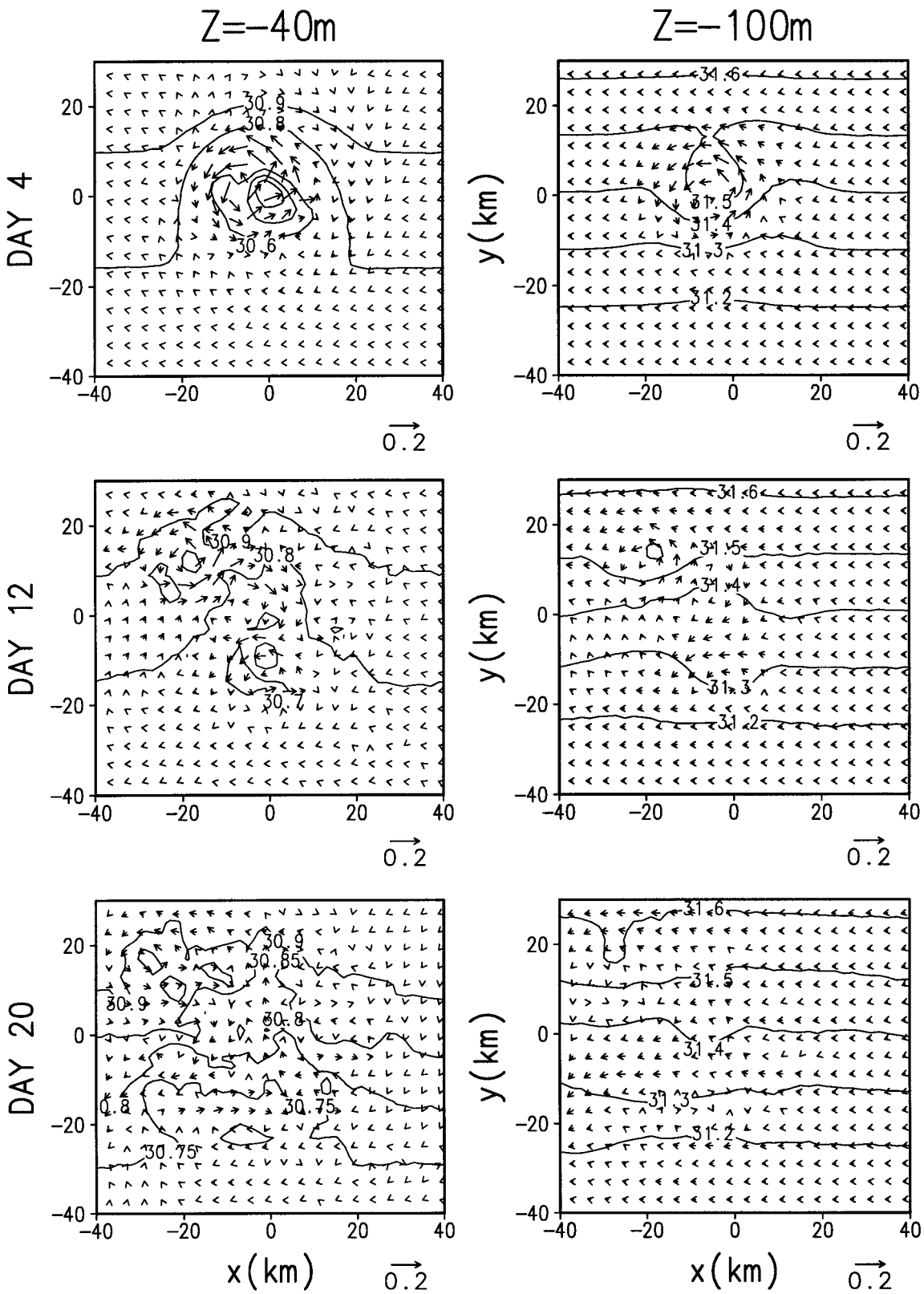

FIG. 9. Flow and salinity (psu) fields near cyclone C1 at depths of 40 m (left) and 100 m (right) at day 4 (top), day 12 (middle), and day 20 (bottom). Calibration arrow is 0.2 m s^{-1}.

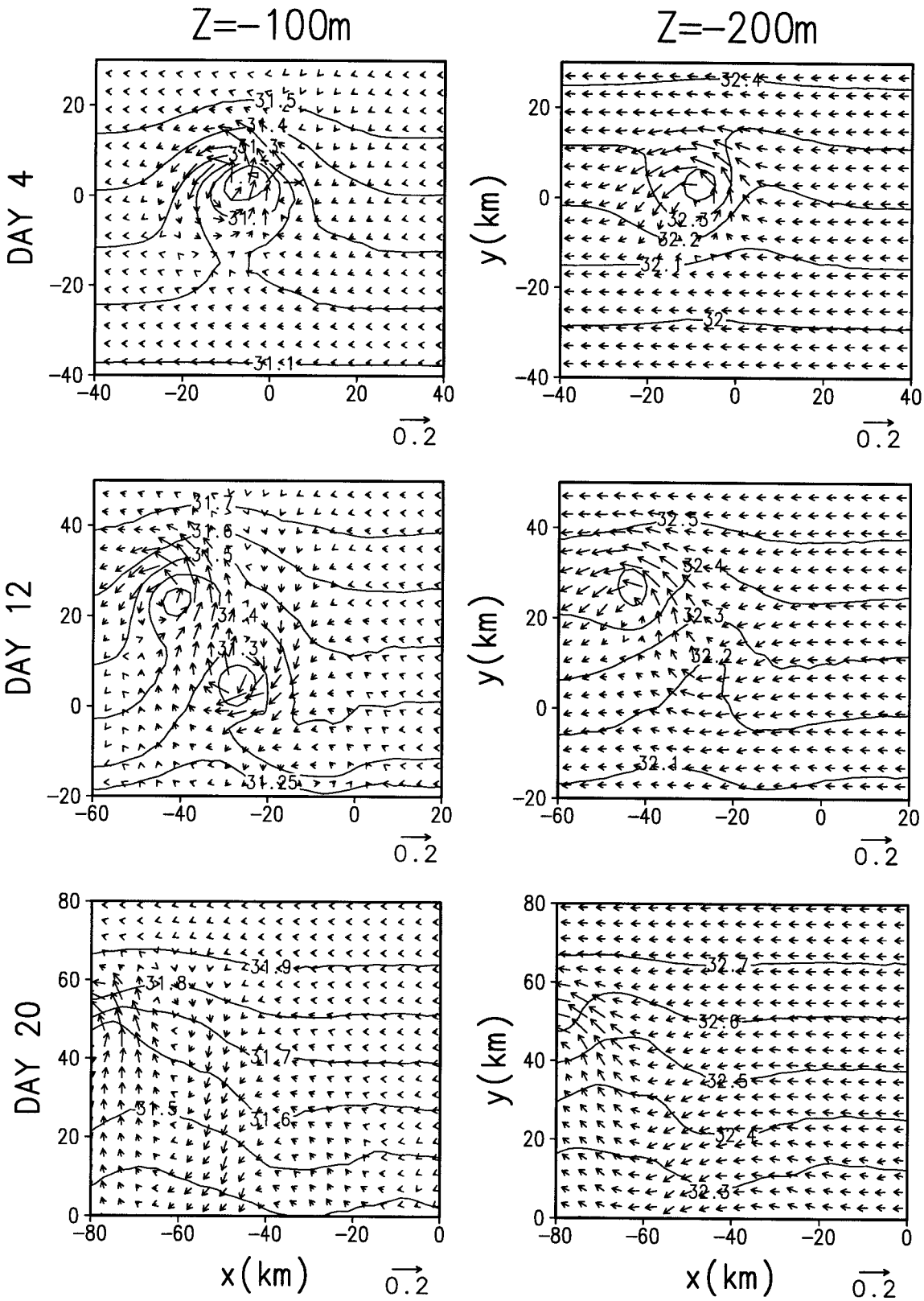

FIG. 10. Same as Fig. 9 but for cyclone C3 at depths of 100 m (left) and 200 m (right). The cyclone has dispersed at day 20.

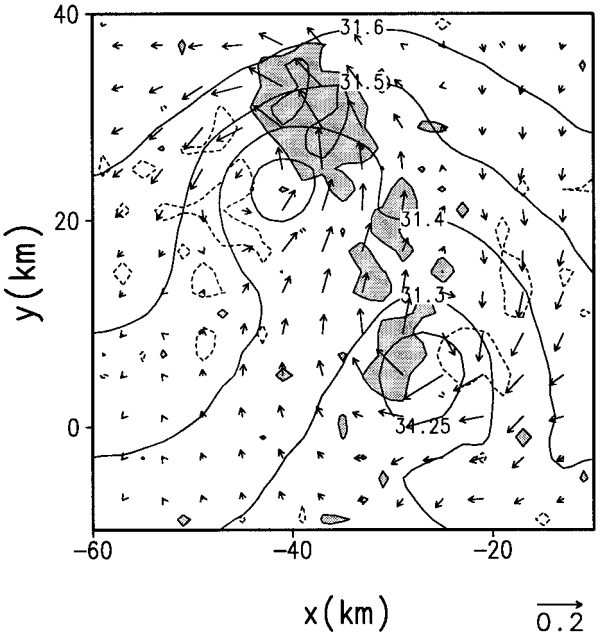

FIG. 11. Vertical velocity at $z = -200$ m superimposed on salinity (psu) and horizontal flow fields at 100 m for cyclone C3 at day 12. Contour lines, shading and calibration arrow length are the same as those in Fig. 8.

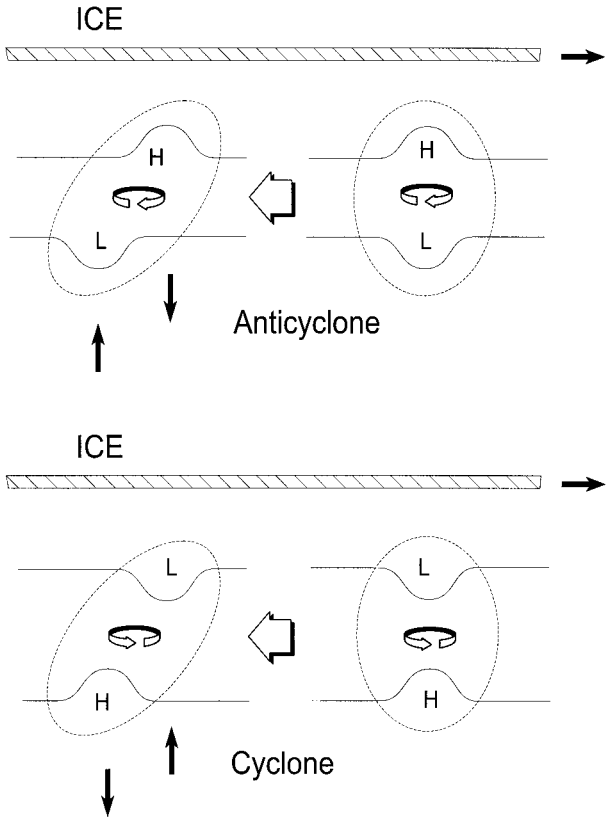

FIG. 12. Schematic side views of eddies experiencing a sudden, large tilt. Vertical velocities are triggered to disperse an anticyclone (top) and a cyclone (bottom). Symbols **H** and **L** denote density surpluses and deficits relative to surrounding waters, respectively.

5. Discussion

A sudden, sizeable tilt destabilizes an eddy. The consequent process leading to its destruction is illustrated schematically in Fig. 12. For an anticyclone in the upright position, effects of the upper-level density surplus and the lower-level deficit cancel when weighing on deep waters below. The pressure surfaces at depths well beneath the eddy are level, and there is no deep current. For a cyclone, the cancellation is between the upper-level density deficit and the lower-level surplus. Submerged eddies owe their stability to the pressure balance at depths.

If a sizeable tilt is suddenly enforced, large vertical velocities will be triggered by the pressure imbalance at depths to disperse the eddy. The process has been analyzed in CS96 as a Rossby adjustment. In essence, the large vertical velocity occurs in the first inertial period, diminishing as the eddy disperses. The transient vertical velocity increases with increasing water depth, decreasing eddy size, and increasing Rossby radii characterizing the upper-ocean stratification. Numerical results in the preceding sections suggest the development of a secondary circulation as a means to prevent the sudden destruction scenario. Eddies disperse away if the secondary circulation fails to keep the upper and lower portions of an eddy from drifting apart.

Figure 13 illustrates schematically circulations associated with a tilted cyclone (top) and anticyclone (bottom) in motion. As before, these circulation patterns are perceived by an ice-based observer. Eddy tilting is exaggerated to ease the illustration. Besides differential advection with depth by the westward current, lateral drift produced by the north–south pressure difference is more pronounced for the lower part of the eddy. The northwestward tilt of a cyclone and the southwestward tilt of an anticyclone are caused by these basic processes. The transverse pressure difference across a moving eddy not only produces the lateral tilt but also builds up a transverse jet in time. Since it takes time for a pressure gradient force to produce a jet, it is plausible that the transverse jet trails behind a moving eddy. The jet is built up by the vertically misaligned pressure ridge and depression as shown in Fig. 12. When the eddy is tilted, salinity surfaces behind a moving anticyclone show coherent southward displacements, which develop into a trough. Similarly, a crest develops behind a cyclone. The crest and trough provide a conduit supporting the narrow jet following the moving eddy.

The lifting force transverse to the ambient flow is stronger in the lower part of the eddy. The jet behind the moving eddy is, however, stronger at depths of the upper half of the eddy. This is clear from all experiments that we have conducted so far. For both cyclones and anticyclones, the jet turns with the swirling flow of an eddy. The veering jet with higher speeds at upper levels

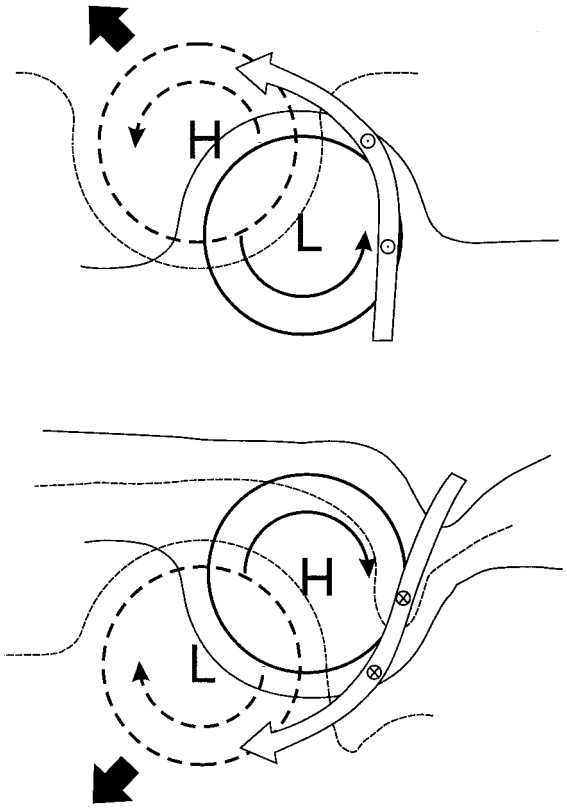

FIG. 13. Schematic plane views of circulations near a tilted cyclone (top) and anticyclone (bottom) in the westward ambient current shown in Fig. 2 from an observer moving with the ice cover. Solid and dashed lines indicate features associated with the upper and lower halves of an eddy, respectively. Density surpluses and deficits are marked by **H** and **L**. Large open arrows with associated upwelling (⊙) and downwelling (⊗) indicate the jet trailing an eddy. Large solid arrows indicate directions of eddy drift relative to ice.

helps the upper part of an eddy to catch up with the lower portion. In all numerical experiments, upper and lower halves of an eddy never drift apart in spite of the constant strain exerted by the sheared current. A sizeable tilt of about half the eddy radius per 100-m depth usually signals eddy dispersal a few days later.

The northward jet carries light water and induces upwelling, while the southward jet advects heavier water and produces downwelling. Upwelling and downwelling generate, respectively, anticyclonic and cyclonic circulations in the upper ocean. For cyclones, the northward jet and the southward return flow farther behind form an overall anticyclonic circulation, which is conceivably caused by upwelling passing through the region at earlier times. For the anticyclone, the southward jet and the return flow farther behind form a cyclonic gyre, apparently manifested by downwelling.

Figure 13 illustrates, to the lowest order, the symmetric nature of circulations associated with a moving cyclone and a moving anticyclone with respect to the axis of the basin. Beyond the first-order symmetry, asymmetry also manifests sizeable differences. Upwelling brings features to the upper ocean in the wake of a moving cyclone; downwelling produces a relatively featureless wake behind a moving anticyclone. Behind a shallow cyclone the wake is diffusive, but a shallow anticyclone forms behind a deeper cyclone and dissipates in time. The life spans for cyclones and anticyclones are also unequal. An anticyclone survives longer in a vertically sheared current than a comparable cyclone does. Forced by a vertically sheared current, cyclones drift into waters where stratification below the sheared layer becomes increasingly weaker. On the other hand, anticyclones enter waters of stronger stratification at the depth of the lower core. Stratification inhibits the development of vertical velocity at the depth of the lower core and prevents eddy dispersal. In experiment A2, decreasing the vertical salinity gradient below 140 m destabilizes the eddy. Therefore, submerged anticyclones owe their longevity to the good fortune of being deflected into increasingly stratified waters by a vertically sheared current.

Mechanisms envisaged herein should not be sensitive to high-frequency fluctuations of ice drifts induced by winds since it takes a long time for the ice drift to induce a deep shear layer. Most of these fluctuations are expected to dissipate or cancel each other before they produce a sizable shear layer extending to a few hundreds of meters below. The present model cannot be applied to interactions of eddies with wind-induced shear layers in open waters. In an open water setting, the top eddy will not dissipate easily. Once disturbed, the vertically stacked pairs as illustrated in Fig. 1 will be more unstable in the baroclinic sense. Further, if a vertically stacked pair is tilted, the two eddies may self-propagate as a pair similar to the heton-type coupling suggested by Hogg and Stommel (1985).

Interactions between subsurface eddies and vertically sheared currents have been examined before. With meddy movements in mind, these models mostly deal with distant interactions between a sheared current aloft and a submerged anticyclone below (Dewar and Meng 1995). The dynamic regime is quite different from the present setting. Of marginal relevance is the work of Walsh (1995), who considered a vertically sheared current in the same depth range of a submerged eddy. His problem was formulated under a quasigeostrophic approximation, and linear solutions were sought. In a steady-state balance, the lateral tilt of a submerged anticyclone in Walsh's model is opposite to our finding. Numerous assumptions in Walsh's analytical model prevent us from making a meaningful comparison. Nevertheless, it should be emphasized that we treat the subject as an initial value problem, in which a suddenly created eddy is subject to advection by a sheared flow. The steady-state balance as envisioned by Walsh was never realized in our model.

6. Conclusions

The consequence of forcing by a mesoscale brine or freshening source under drifting ice has been examined.

Shallow axisymmetric brine and freshening sources generate submerged anticyclones and cyclones, respectively. Drifting with the ice cover, an eddy is subject to differential advection by the vertically sheared current induced by the ice drift. It may be argued that a localized freshening source extending to considerable depths may not be nature's way to produce cyclones under sea ice. It nevertheless provides an effective means to produce submerged cyclones and to contrast the difference between submerged cyclones and anticyclones. The study focuses on a range of parameters in which the ambient current and the eddy circulation have comparable strength and vertical scales. Other limits are not so interesting. Two of them are degenerate: a vanishing ice drift and a depth scale of the sheared current much larger than the vertical scale of an eddy. In these cases, a stable eddy experiences little ambient currents and is subject to slow viscous dissipation. Fast spinning eddies are expected to survive the weak current shear induced by the ice drift. Very weak eddies are subject to fast dispersal by a vertically sheared current. Leaving the uninteresting limits aside, major conclusions are summarized below.

A sheared current in the vertical disperses eddies through differential advection with depth. Eddies of either polarity are advected not only in the direction of the stream but also laterally. When an eddy is embedded in a horizontally uniform current, speed difference across the eddy induces a pressure gradient force, which in turn produces the lateral drift. Independent of the hemisphere, an ice-based observer facing upstream of the ice drift would find that clockwise and counterclockwise rotating eddies are deflected to the left and right, respectively. This point was verified in our preliminary experiments. The dynamics leading to the lateral deflection is akin to the Kutta–Zhukhovski lift theorem governing potential flows past a cylinder with circulation around it. The age-old theorem, seemingly too simplistic, transcends a vast parameter space including the earth's rotation, flow divergence, baroclinicity, and finite-amplitude nonlinearity. Deviations from the theory are minor.

Relative to the ice drift, the backward and lateral motion is faster for the lower portion of an eddy. A jet develops pointing to and following the movement of a tilted eddy. The elevated jet core apparently helps the upper part of the eddy to accelerate toward the lower half of the eddy and in the process reduces the strain exerted by the vertical shear of the ambient current. Eddies disperse in time if the jet fails to prevent a sizeable tilt; this happens if the vertical shear of the ambient current is too strong or if the halocline is much elevated. In this light, the abundance of submerged eddies under ice cover should not be taken for granted. These eddies owe their longevity to a slow ice drift and a strong halocline at the depth of the eddy. In regions of rapid ice drift and weak stratification, these eddies are expected to disperse quickly.

In line with observations, our case against the survivability of submerged cyclones under Arctic ice is still mounting. To begin, a mesoscale brine source under sea ice is physically more plausible than a localized freshening source, which favor the production of submerged anticyclones. Unlike a brine source, a freshening source is likely to spread horizontally rather than to accumulate locally to considerable depths. Even if one takes the extreme view that mesoscale brine and freshening sources are equally probable, anticyclones are still favored over cyclones. It would take a much deeper freshening source and more freshwater content over the volume to produce a submerged cyclone with strength and dimensions comparable to an anticyclone. The sheared current under drifting ice provides another account against the survival of subsurface cyclones. Embedded in a geostrophically balanced sheared current under drifting ice, cyclones and anticyclones are deflected into waters with weaker and stronger haloclines, respectively. Vertical motion is less inhibited in weak haloclines, destroying submerged cyclones.

It seems too early to tell whether the three accounts against submerged cyclones are adequate to explain the overwhelming predominance of anticyclones under Arctic ice. Not enough processes have been assessed by qualified models to make an informed judgment. Presently, we do not know whether most eddies are generated in open waters and subsequently run over by the ice cover or are produced locally. Models to assess the survivability of eddies moving in and out of regions covered by ice are still wanting. Even after all these efforts are rendered, merging of all processes will not be complete before polarity tests can be conducted for a group of eddies moving in and out of marginal ice zones. This paper is a small step toward the long quest.

Acknowledgments. The authors were supported by the Arctic Sciences Section, Office of Polar Programs of the National Science Foundation under Grants OPP-9709952 and OPP-9614107, respectively.

REFERENCES

Blumberg, A. F., and G. L. Mellor, 1987: A description of a three-dimensional coastal ocean circulation model. *Three-Dimensional Coastal Ocean Models,* N. S. Heaps, Ed., Amer. Geophys. Union, 1–16.

Chao, S.-Y., and P.-T. Shaw, 1996: Initialization, asymmetry, and spindown of Arctic eddies. *J. Phys. Oceanogr.,* **26,** 2076–2092.

Cushman-Roisin, B., and B. Tang, 1990: Geostrophic turbulence and emergence of eddies beyond the radius of deformation. *J. Phys. Oceanogr.,* **20,** 97–113.

D'Asaro, E. A., 1988: Generation of submesoscale vortices: A new mechanism. *J. Geophys. Res.,* **93,** 6685–6693.

Dewar, W. K., and H. Meng, 1995: The propagation of submesoscale coherent vortices. *J. Phys. Oceanogr.,* **25,** 1745–1770.

Dixit, B., 1978: Some mesoscale flow features in the Beaufort Sea during AIDJEX 75–76. Ph.D. dissertation, McGill University, 244 pp.

Galt, J. A., 1967: Current measurements in the Canada Basin of the

Arctic Ocean, Summer 1965. Tech. Rep. 184, University of Washington, Seattle, 17 pp.
Hogg, N. C., and H. M. Stommel, 1985: The heton: An elementary interaction between discrete baroclinic geostrophic vortices and its implications concerning eddy heat-flow. *Proc. Roy. Soc. London,* **A397,** 1–20.
Kundu, P. K., 1990: *Fluid Mechanics.* Academic Press, 638 pp.
Manley, T. O., and K. Hunkins, 1985: Mesoscale eddies of the Arctic Ocean. *J. Geophys. Res.,* **90,** 4911–4930.
Mellor, G. L., and T. Yamada, 1974: A hierarchy of turbulence closure models for planetary boundary layers. *J. Atmos. Sci.,* **31,** 1791–1806.
Newton, J., 1973: The Canada Basin: Mean circulation and intermediate-scale flow features. Ph.D. dissertation, University of Washington, Seattle, 158 pp.
Nof, D., 1989: Why are there more anticyclones than cyclones in the Arctic Ocean? *Proc. Regional and Mesoscale Modeling of Ice Covered Oceans,* Bergen, Norway, International Association for Physical Sciences of the Ocean, 29–32.
Smagorinsky, J., 1963: General circulation experiments with the primitive equations. I. The basic experiment. *Mon. Wea. Rev.,* **91,** 99–164.
Walsh, D., 1995: A model of a mesoscale lens in large-scale shear. Part I: Linear calculations. *J. Phys. Oceanogr.,* **25,** 735–746.